Adaptive optics confocal microscopy using direct wavefront sensing

Xiaodong Tao,[1,*] Bautista Fernandez,[1] Oscar Azucena,[1] Min Fu,[2] Denise Garcia,[2] Yi Zuo,[2] Diana C. Chen,[3] and Joel Kubby[1]

[1]Jack Baskin School of Engineering, University of California, Santa Cruz, 1156 High Street MS:SOE2, Santa Cruz, California 95064, USA

[2]Molecular, Cell, and Developmental Biology, University of California, Santa Cruz, 1156 High Street, Santa Cruz, California 95064, USA

[3]Lawrence Livermore National Laboratory, 7000 East Avenue, Livermore, California 94550, USA

*Corresponding author: taoxd@soe.ucsc.edu

Received November 30, 2010; revised February 6, 2011; accepted February 22, 2011; posted February 23, 2011 (Doc. ID 138976); published March 17, 2011

Optical aberrations due to the inhomogeneous refractive index of tissue degrade the resolution and brightness of images in deep-tissue imaging. We introduce a confocal fluorescence microscope with adaptive optics, which can correct aberrations based on direct wavefront measurements using a Shack–Hartmann wavefront sensor with a fluorescent bead used as a point source reference beacon. The results show a 4.3× improvement in the Strehl ratio and a 240% improvement in the signal intensity for fixed mouse tissues at depths of up to 100 μm.

OCIS codes: 110.1080, 010.7350, 180.2520, 180.6900, 170.3880.

The ideal imaging performance of a confocal microscope in terms of resolution and imaging depth can rarely be achieved in most applications. Variation in the refractive index from the inhomogeneous optical properties of biological samples and the interface between the sample and mounting medium distorts the light and degrades the final image. Compared with the wide-field microscope, the confocal microscope suffers from more aberrations because both the excitation and emission light are distorted when they go though the sample [1]. The distortion in excitation light decreases the intensity of the fluorescent emission light. Using a higher power laser to compensate this effect will cause phototoxicity and photobleaching [2]. Both of these distortions also reduce the resolution of the system. A similar issue was found in astronomy, where the aberrations induced by atmospheric turbulence degrade the final image [3,4]. The wavefront sensor has been applied to measure wavefront distortion directly. However, wavefront sensors often need a reference point source, such as a natural or laser guide star [3,4], which is difficult to realize in the microscope. Because of this, most of the existing adaptive optics (AO) confocal microscopes developed so far are based on indirect methods of wavefront measurement [5,6], which often require numerous iterations. That causes photobleaching and limits the bandwidth for live imaging. Backscattered light has been used for direct wavefront sensing [7]. It is highly dependent on the backscattering efficiency of the tissue. In vision science, retinal lipofuscin autofluorescence [8] or the fluorescently labeled cells in the retina [9] are used for wavefront measurement. A fluorescent microsphere was used for measurement of the 3D point spread function of a microscope [10]. A spherical particle was used as an artificial point source for wavefront measurement [11]. The transmitted illumination used in this approach is not suitable for a laser scanning confocal microscope.

While other research programs are attempting to integrate AO in microscopy, to our knowledge, no other research group uses artificial reference beacons and wavefront sensing in a fluorescent confocal microscope with AO to directly measure the wavefront error. In the proposed system, the wavefront is measured directly by a Shack–Hartmann wavefront sensor (SHWS) with fluorescent microspheres embedded in the sample for use as reference beacons [12]. A separate laser channel is added to excite the microsphere, which shares the same light path with the imaging channel without much of an increase in system complexity. The excitation and emission wavelengths of the fluorescent microsphere were selected specifically to minimize the cross talk between the wavefront sensing channel and the imaging channel, which reduces phototoxicity and photobleaching. Because microspheres can be injected into the tissue *in vivo* [13], this method becomes a viable solution for wavefront correction in live imaging. The current system setup includes two laser channels, an He–Ne laser ($\lambda = 633$ nm), and a solid-state laser ($\lambda = 515$ nm) used for wavefront sensing and fluorescence imaging, respectively (Fig. 1). The emission light from the microsphere

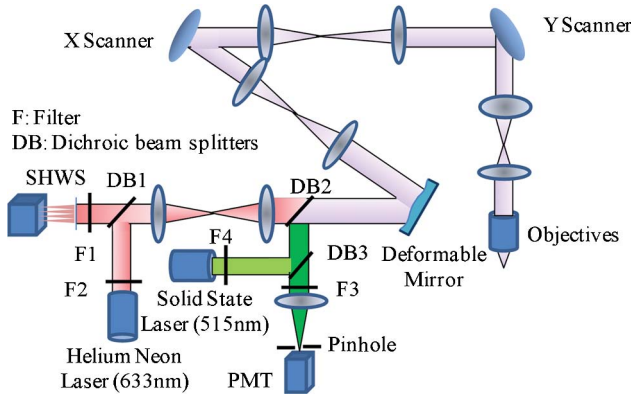

Fig. 1. (Color online) AO confocal microscope: an He–Ne laser emits light at 633 nm for excitation of the fluorescent reference beacons. Light emitted from the reference beacon is passed through filter F1 to the wavefront sensor. A solid-state laser emits light at 515 nm that excites the YFP bred into the sample. The emission light is filtered by F3 and detected by the photomultiplier tube (PMT). The wavefront aberrations are corrected by the DM.

and the sample is collected by an objective lens (×60 water objective, NA 1.2, Olympus) and separated by a dichroic mirror. The light from the microsphere is fed into the SHWS, which is composed of a 44×44 element lenslet array with a lenslet diameter of $400\,\mu$m and focal length of 24 mm (AOA, Inc., Cambridge, Mass.) and an electron-multiplying CCD camera (Photometrics). Because of page limitations, the detailed procedure for the wavefront sensing is referred to in [12]. In the current system, the emission light from the $1\,\mu$m microsphere is stable enough to be detected by the use of a SHWS without photobleaching during the wavefront correction. A smaller microsphere and the phototoxcity effect will be investigated in future research. A deformable mirror [(DM) Boston Micromachines] with 140 actuators and $3.5\,\mu$m of stroke is placed in the optical path, which is conjugate to the exit pupil of the objective and the wavefront sensor. Because of the excitation and emission light sharing the same path, the DM can correct the aberrations on both paths. With the correction information from the wavefront sensor, a direct slope algorithm was applied to control the DM in a closed loop [14]. The wavefront sensor takes 35 ms for each measurement. The closed loop bandwidth is approximately 3 Hz. AO correction was made for the entire scan field rather than pixel by pixel. The isoplanatic half-width defines the size of field of view that the AO system can correct, which is $19\,\mu$m for a *Drosophila* embryo [12]. We will evaluate it for brain tissue in future research. The confocal imaging system has a frame rate of 30 frames/s for live imaging. A science camera captures a fluorescent image of the microspheres for locating a reference beacon.

To test our system, a fixed brain slice from a transgenic mouse with yellow fluorescent protein (YFP) was prepared. Crimson fluorescent microspheres of $1\,\mu$m diameter (Invitrogen, Carlsbad, Calif.) were deposited onto a glass slide and a cover plate for use as laser guide stars. The peak excitation and emission wavelengths are 625 and 645 nm, respectively. Sample brain sections of different thicknesses (15, 50, and $100\,\mu$m) are mounted on the microsphere coated glass slide. The spherical aberration induced from the cover glass was initially compensated by adjustment of a correction collar on the objective lens. The system aberration was further corrected by the DM. To avoid correcting the defocus when the microsphere is out of the focus plane, the AO loop was turned on only when the microsphere is within the depth of field, which can be determined by the defocus aberration measured from the SHWS [14].

The experimental results for the $100\,\mu$m thick section are discussed here for the sake of brevity. The motorized Z stage under the sample focuses the He–Ne laser on the bottom of the tissue. The SHWS then measures the wavefront with the emission light from the microsphere. The rms wavefront error is 0.24λ before correction [Fig. 2(a)]. It suffers from a large amount of spherical aberration. The image of a microsphere from the science camera is very dim [Fig. 2(c)]. After turning on the DM, the rms wavefront error converges after 10 iterations. The rms wavefront error decreased to 0.028λ [Fig. 2(b)]. The corrected wavefront provides a much brighter image [Fig. 2(d)]. The Strehl ratio was measured using the method described in [12] at 10 different positions on each sample (Table 1). The improvement in the Strehl ratio was approximately 4.3× for a $100\,\mu$m thick sample.

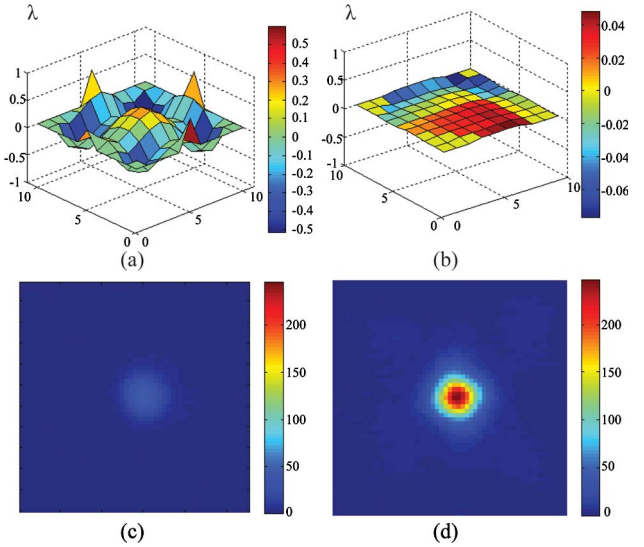

Fig. 2. (Color online) Wavefront measurements from a fluorescent microsphere. Wavefront error (a) before and (b) after correction. The rms errors for (a) and (b) are 0.24λ and 0.028λ ($\lambda = 633$ nm), respectively. Images of the microsphere (c) before and (d) after correction.

Confocal fluorescence images of the brain tissues are achieved with and without correction. The sectioned images are collected by scanning the focal plane from the bottom of the tissue up with $3\,\mu$m steps in the Z direction. The size of the image is $51.8\,\mu\text{m} \times 51.8\,\mu$m. The object size corresponding to a pixel is 101 nm. Before correction, it is hard to observe the dendrite and spine around the cell body in the maximum intensity projection image [Fig. 3(a)]. The enlarged region in the dashed box is shown in Fig. 3(c) with normalized display intensity. It is difficult to distinguish between the signal and background noise. After correction by the DM, intensity and contrast are improved. The same area was enlarged, which gives a clear image of the dendrite [Fig. 3(d)]. The profiles of the lines along the dendrite in Figs. 3(c) and 3(d) are shown in Fig. 3(e). The intensity increases by 240% after the wavefront correction. 3D volume images are then generated from sectioned images using ImageJ (National Institutes of Health, Bethesda, Md.). The enlarged views in the solid box in Figs. 3(a) and 3(b) show great improvement after the wavefront error has been corrected [Figs. 4(a) and 4(b), Media 1 and Media 2]. For the sample tissues with thicknesses of 25 and $50\,\mu$m, the intensity increased by 30% and 43%, respectively. The transverse and axial resolution for the $50\,\mu$m thick tissue was improved from

Table 1. Statistical Properties of the Strehl Ratio for Brain Tissues

No.	Thickness (μm)	Strehl Ratio before Correction		Strehl Ratio after Correction	
		Mean	Std. Dev.	Mean	Std. Dev.
1	15	0.718	0.020	0.995	0.003
2	50	0.515	0.026	0.978	0.011
3	100	0.224	0.038	0.964	0.018

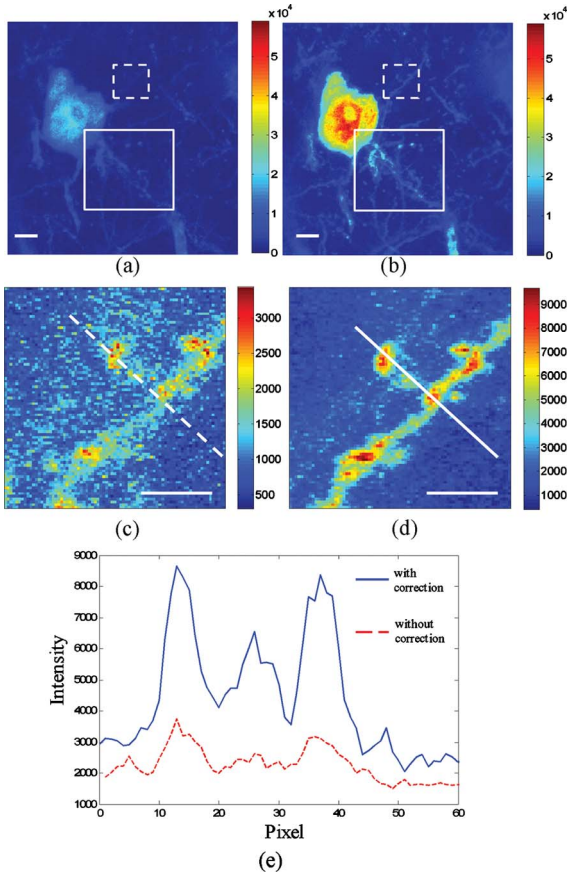

Fig. 3. (Color online) Confocal fluorescence imaging through 100 μm thick mouse brain tissue. The maximum intensity projection image from the bottom of the tissue (a) before and (b) after correction. The dashed boxes indicate the enlarged image (c) before and (d) after correction. (e) Intensity profiles along the dashed curve in the uncorrected image (c) and along the solid curve in the corrected image (d). The scale bar is 5 μm.

0.29 to 0.26 and 0.74 to 0.64 μm, respectively. The highly scattering *Drosophila* embryo was also tested. The improvement of the Strehl ratio was 2.32×.

To obtain an image with the same intensity as a standard confocal microscope, the proposed system could have a shorter exposure time during confocal imaging. The exposure time during wavefront sensing in the current system is only 0.35 s, which is much shorter than the indirect wavefront method (>30 s in [5]). All these factors reduce the possibility of phototoxicity and photobleaching. They also enable a higher speed of imaging for dynamic live samples. To correct the aberrations from thicker tissue, the microsphere could be injected into the mouse brain at a different depth. By correcting the aberration from the top to the bottom gradually, the wavefront sensor may capture more light from the microsphere using the previous correction on the DM.

To compare our system performance with a standard commercial confocal system (Leica TCS SP5 II), the resolution was investigated for a 50 μm thick brain tissue sample on both systems using objective lenses with the same NA (1.2) and detectors with the same size pinholes (0.9 Airy units). The transverse/axial resolutions were

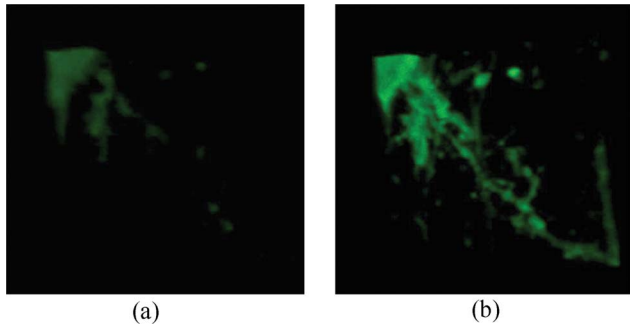

Fig. 4. (Color online) Enlarged 3D volume images of solid box in Fig. 3 (a) before (Media 1) and (b) after correction (Media 2).

increased from 0.32/1.42 for the commercial system to 0.23 μm/0.8 μm for our AO system after correction. Although reducing the pinhole diameter can increase the resolution, the commercial system still suffers from aberrations. The lateral/axial resolution for the commercial system with 0.5 Airy units is 0.29 μm/1.11 μm.

In conclusion, with the use of direct wavefront measurements by a SHWS and corrections from a DM, the aberrations can be measured and corrected accurately at high speed, which shows its potential ability for live *in vivo* imaging. The effects to the functionality of a neuron in live brain tissue for microsphere injection will be investigated in the future.

This work was supported by the National Science Foundation (NSF) (0852742). The authors acknowledge Claire Max at the Center for Adaptive Optics, Donald Gavel and Daren Dillon at the Laboratory for Adaptive Optics, and Yu-Chen Hwang from the Life Sciences Microscopy Center, University of California, Santa Cruz.

References

1. J. B. Pawley, *Handbook of Biological Confocal Microscopy* (Springer, 2006).
2. M. J. Booth, Phil. Trans. R. Soc. A **365**, 2829 (2007).
3. R. K. Tyson, *Principles of Adaptive Optics* (Academic, 1991).
4. H. W. Babcock, Publ. Astron. Soc. Pac. **65**, 229 (1953).
5. P. Marsh, D. Burns, and J. Girkin, Opt. Express **11**, 1123 (2003).
6. N. Ji, D. E. Milkie, and E. Betzig, Nat. Meth. **7**, 141 (2010).
7. M. Rueckel, J. A. Mack-Bucher, and W. Denk, Proc. Natl. Acad. Sci. USA **103**, 17137 (2006).
8. L. Diaz, S. Haro, and J. C. Dainty, Opt. Lett. **24**, 61 (1999).
9. D. P. Biss, D. Sumorok, S. A. Burns, R. H. Webb, Y. Zhou, T. G. Bifano, D. Côté, I. Veilleux, P. Zamiri, and C. P. Lin, Opt. Lett. **32**, 659 (2007).
10. J. L. Beverage, R. V. Shack, and M. R. Descour, J. Microsc. **205**, 61 (2002).
11. M. Reicherter, W. Gorski, T. Haist, and W. Osten, Proc. SPIE **5462**, 68 (2004).
12. O. Azucena, J. Crest, J. Cao, W. Sullivan, P. Kner, D. Gavel, D. Dillon, S. Olivier, and J. Kubby, Opt. Express **18**, 17521 (2010).
13. P. Menei, A. Croue, V. Daniel, A. Pouplard-Barthelaix, and J. P. Benoit, J. Biomed. Mater. Res. **28**, 1079 (1994).
14. J. Porter, H. Queener, J. Lin, K. Thorn, and A. A. S. Awwal, *Adaptive Optics for Vision Science: Principles, Practices, Design and Applications* (Wiley, 2006).